Inverse Problems, Design and Optimization Symposium
Rio de Janeiro, Brazil, 2004

Localization of Unexploded Ordnances (UXOs) with Magnetic Field Measurements

Bernhard Brandstätter
Christian Doppler Laboratory for Automotive Measurement Research
located at the
Institute of Electrical Measurement and Measurement Signal Processing
Graz University of Technology, Austria
brand@ieee.org

ABSTRACT

In this paper a novel method to reconstruct the location an the orientation of unexploded ordnances (UXO's) by means of a two stage reconstruction process is presented. The first stage consists of obtaining a rough reconstruction based on magnetic field signatures at the earth's surface, while in the second stage the results from the first steage are going to be improved. For the reconstruction a Gauss-Newton method with analytical Jacobians is being used.

INTRODUCTION

The four major categories of technologies for the detection of UXO are magnetometry, infrared (IR), ground penetrating radar (GPR) and electrical impedance measurement (EIM). Magnetometers (fluxgate or cesium vapor) are the most commonly used form of detecting UXO on or below the surface and can be applied for underwater use. Magnetometers can only detect UXOs containing ferrous metal. Metal detectors (making use of eddy currents) can locate both ferrous and nonferrous metallic objects and can be adapted for underwater use, as well; however, conventional metal detectors can only detect UXOs located on or very near the surface. Infrared has proven effective only in conducting gross assessments of areas containing UXOs, but lacks the capability to provide point detection of UXOs. GPR and EIM can collect rough images of buried metallic and nonmetallic UXO. GPR effectiveness is severely limited in certain soil conditions.

Magnetic detection (the method discussed in this section) is a widely used method for the location and identification of unexploded ordnances (UXO). The presence of ordnances results in magnetic anomalies superimposed on the background geomagnetic field [1].

The current state of the art is to model these magnetic anomalies by means of a magnetic dipole ([2], [3], [4], [5]), whose field is superimposed to the earth magnetic field leading to a fast reconstruction of the bomb location, but little information can be drawn from that model what shape and orientation of the UXO is concerned.

Sometimes in UXO detection it might be helpful to know not only the depth of the object but also the orientation and size. To perform this type of reconstruction we may approximate the ordnance with a prolate spheroid for which we are able to obtain an analytical solution.

Consider the situation of Fig. 1, where a spheroid is buried in earth. The location and shape of the spheroid are given by x_0, y_0, z_0, Θ (the angle between the semi major axis of the spheroid and z-axis), ϕ (angle between axis of the spheroid and x-axis), b and c. The geomagnetic field is given by B_{x0}, B_{y0} and B_{z0}.

The forward problem is to calculate the magnetic flux density at the earth's surface. Then the spheroidal model is varied until the measurement data (measured magnetic flux density at the earth's

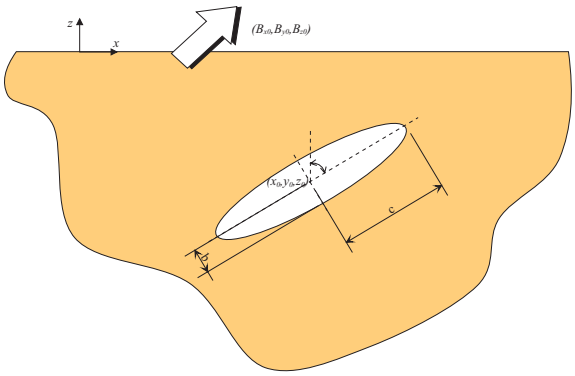

Figure 1: Buried unexploded ordnance approximated with a prolate spheroid. The location and shape of the spheroid are given by x_0, y_0, z_0, Θ (the angle between the semi major axis of the spheroid and z-axis), ϕ (angle between axis of the spheroid and x-axis), b and c. The geomagnetic field is given by B_{x0}, B_{y0} and B_{z0}.

surface) meet the calculated magnetic flux density resulting from the spheroidal model.

ANALYTICAL SOLUTION OF THE FORWARD PROBLEM

This problem can be solved best by introducing elliptical coordinates:

$$\begin{array}{l} x = a\,sinh(\eta)\,sin(\vartheta)\,cos(\psi) \\ y = a\,sinh(\eta)\,sin(\vartheta)\,sin(\psi) \\ z = a\,cosh(\eta)\,cos(\vartheta) \end{array} , \qquad (1)$$

where $b = a\,sinh(\eta)$, $c = a\,cosh(\eta)$, $0 \leq \eta \leq \infty$, $0 \leq \vartheta \leq \pi$ and $0 \leq \psi \leq 2\pi$. $\vartheta = const.$ refers to hyperboloids, $\eta = const.$ to prolate spheroids and $\psi = const.$ to meridian planes.

Due to the fact that we do not have a current density in the domain of interest, allows us to introduce a magnetic scalar potential V_m

$$\nabla \times \vec{H} = 0 \Rightarrow \vec{H} = -\nabla V_m. \qquad (2)$$

The geomagnetic field is expressed as an intrinsic magnetic scalar potential V_e

$$V_e = -\frac{1}{\mu_0}\left[B_{x0}x + B_{y0}y + B_{z0}z\right] + K, \qquad (3)$$

where K is some constant and μ_0 is the permeability of vacuum.

The differential equation for V_m that has to be fulfilled can be obtained once again from Maxwell's equations

$$\vec{H} = -\nabla\Phi_m, \nabla\vec{B} = 0 \Rightarrow \triangle\Phi_m = 0. \qquad (4)$$

Or in elliptic coordinates

$$\begin{array}{l} \frac{1}{a^2(sinh^2\eta + sin^2\vartheta)}\left\{\frac{\partial^2\Phi_m}{\partial\eta^2} + coth\,\eta\frac{\partial\Phi_m}{\partial\eta}\right. \\ \left. + \frac{\partial^2\Phi_m}{\partial\vartheta^2} + cot\,\vartheta\frac{\partial\Phi_m}{\partial\vartheta}\right\} \\ + \frac{1}{a^2 sinh^2\eta\, sin^2\vartheta}\frac{\partial^2\Phi_m}{\partial\psi^2} = 0. \end{array} \qquad (5)$$

The general solution for (5) can be obtained by means of separation of variables

$$\begin{array}{l} V_m = \sum_{q=0}^{\infty}\sum_{n=0}^{\infty}\left\{\left[\alpha_{1qn}P_q^n(cosh\,\eta)\right.\right. \\ \left. + \alpha_{2qn}Q_q^n(cosh\,\eta)\right] \\ \left[\alpha_{3qn}P_q^n(cos\,\vartheta) + \alpha_{4qn}Q_q^n(cos\,\vartheta)\right] \\ \left.\left[\alpha_{5qn}sin(n\psi) + \alpha_{6qn}cos(n\psi)\right]\right\}, \end{array} \qquad (6)$$

where P and Q are Legendre polynomials.

The boundary and interface conditions (between the ferromagnetic spheroid (region 1) and earth (region (2)) that have to be fulfilled are

$$\begin{array}{l} V_{m,1} = V_{m,2} \\ \mu_1\frac{\partial V_{m,1}}{\partial n} = \mu_2\frac{\partial V_{m,2}}{\partial n} \\ \eta \to \infty : V_{m,2} = V_e, \end{array} \qquad (7)$$

where n is the normal vector.

Due to the fact that $Q(1) \to \infty$, the terms in the general solution containing $Q(cos\,\vartheta)$ have to be eliminated.

Since $\eta \to \infty : V_{m,2} = V_e$ we know that $n = 0, 1$ because $cos(n\psi)$ and $sin(n\psi)$ occur only with $n = 1$ in (3).

Additional due to the properties of P (and comparison with (3)) it follows that $q = 0, 1$ too.

In the following we assume that in the whole region 2 permeability of vacuum is valid ($\mu_2 = \mu_0$).

Considering the interface conditions, one finally ends up with the solution in domain 2 (the

one in which we are interested in)

$$\begin{array}{l}\Phi_2 = K - \frac{B_{z0}a}{\mu_2}cosh(\eta)cos(\vartheta) - \\ \frac{B_{y0}a}{\mu_2}sinh(\eta)sin(\vartheta)sin(\psi) - \\ \frac{B_{x0}a}{\mu_2}sinh(\eta)sin(\vartheta)cos(\psi) + \\ \frac{B_{z0}asinh(\eta_0)\frac{1}{\mu_2}(\mu_{r1}-1)Q_1^0(cosh(\eta))cos(\vartheta)}{\frac{\mu_{r1}Q_1^0(cosh(\eta_0))}{coth(\eta_0)} - Q_1^{0'}(cosh(\eta_0))sinh(\eta_0)} + \\ \frac{B_{y0}acosh(\eta_0)\frac{1}{\mu_2}(\mu_{r1}-1)Q_1^1(cosh(\eta))sin(\vartheta)sin(\psi)}{\frac{\mu_{r1}Q_1^1(cosh(\eta_0))}{tanh(\eta_0)} - Q_1^{1'}(cosh(\eta_0))sinh(\eta_0)} + \\ \frac{B_{x0}acosh(\eta_0)\frac{1}{\mu_2}(\mu_{r1}-1)Q_1^1(cosh(\eta))sin(\vartheta)cos(\psi)}{\frac{\mu_{r1}Q_1^1(cosh(\eta_0))}{tanh(\eta_0)} - Q_1^{1'}(cosh(\eta_0))sinh(\eta_0)},\end{array} \tag{8}$$

with

$$\begin{array}{l}Q_1^0(x) = Q_1(x) = \frac{x}{2}\ln\left(\frac{x+1}{x-1}\right) - 1 \\ Q1^{0'} = \frac{d}{dx}Q_1^0(x) \\ Q_1^1(x) = \left(x^2-1\right)^{\frac{1}{2}}\frac{d}{dx}Q_1(x) \\ Q1^{1'} = \frac{d}{dx}Q_1^1(x)\end{array} \tag{9}$$

μ_{r1} is the relative permeability of the ferromagnetic UXO and $\eta = \eta_0$ denotes the interface between region 1 and region 2 (i. e. the surface of the UXO).

In (8) there is still a constant K remaining which is irrelevant, since we are interested in calculating the magnetic flux density

$$\begin{array}{l}B'_x = -\mu_0\left(\nabla V_2\right)_x = -\mu_0\left[\frac{1}{a^2(sinh^2(\eta)+sin^2(\vartheta))}\right. \\ \Big(a\,cosh(\eta)sin(\vartheta)cos(\psi)\frac{\partial V_2}{\partial\eta} + \\ a\,sinh(\eta)cos(\vartheta)cos(\psi)\frac{\partial V_2}{\partial\vartheta}\Big) - \\ \left.\frac{1}{a^2sinh^2(\eta)sin^2(\vartheta)}a\,sinh(\eta)sin(\vartheta)sin(\psi)\frac{\partial V_2}{\partial\psi}\right] \\ B'_y = -\mu_0\left(\nabla V_2\right)_y = -\mu_0\left[\frac{1}{a^2(sinh^2(\eta)+sin^2(\vartheta))}\right. \\ \Big(a\,cosh(\eta)sin(\vartheta)sin(\psi)\frac{\partial V_2}{\partial\eta} + \\ asinh(\eta)cos(\vartheta)sin(\psi)\frac{\partial V_2}{\partial\vartheta}\Big) + \\ \left.\frac{1}{a^2sinh^2(\eta)sin^2(\vartheta)}a\,sinh(\eta)sin(\vartheta)cos(\psi)\frac{\partial V_2}{\partial\psi}\right] \\ B'_z = -\mu_0\left(\nabla V_2\right)_z = -\mu_0\left[\frac{1}{a^2(sinh^2(\eta)+sin^2(\vartheta))}\right. \\ \left.\Big(a\,sinh(\eta)cos(\vartheta)\frac{\partial V_2}{\partial\eta} - acosh(\eta)sin(\vartheta)\frac{\partial V_2}{\partial\vartheta}\Big)\right]\end{array} \tag{10}$$

For calculating the derivatives $\frac{\partial V_2}{\partial\eta}$, $\frac{\partial V_2}{\partial\vartheta}$ and $\frac{\partial V_2}{\partial\psi}$ the following abbreviations are used

$$C_{10} = \frac{B_{z0}\,a\,sinh(\eta_0)\frac{\mu_{r1}-1}{\mu 0}}{\frac{\mu_{r1}Q_1^0(cosh(\eta_0))}{coth(\eta_0)} - Q_1^{0'}(cosh(\eta_0))sinh(\eta_0)} \tag{11}$$

and

$$\widetilde{C_{11}} = \frac{\vec{B_0}\,a\,cosh(\eta_0)\frac{\mu_{r1}-1}{\mu 0}}{\frac{\mu_{r1}Q_1^1(cosh(\eta_0))}{tanh(\eta_0)} - Q_1^{1'}(cosh(\eta_0))sinh(\eta_0)}, \tag{12}$$

Then (8) simplifies to

$$\begin{array}{l}V_2 = K - \frac{B_{z0}a}{\mu_0}cosh(\eta)cos(\vartheta) - \\ \frac{B_{y0}a}{\mu_0}sinh(\eta)sin(\vartheta)sin(\psi) - \\ \frac{B_{x0}a}{\mu_2}sinh(\eta)sin(\vartheta)cos(\psi) + \\ C_{10}Q_1^0(cosh(\eta))cos(\vartheta) + \widetilde{C_{11}}sin(\vartheta)\left(\vec{e_y}sin(\psi) + \right. \\ \left.\vec{e_x}cos(\psi)\right)Q_1^1(cosh(\eta))\end{array} \tag{13}$$

which leads to concise expressions for the derivatives

$$\begin{array}{rcl}\frac{\partial V_2}{\partial\eta} = & -\frac{\vec{B_0}a}{\mu_0}\left(\vec{e_z}sinh(\eta)cos(\vartheta) + \right. & \\ & \left. cosh(\eta)sin(\vartheta)\right. & \\ & \left.(\vec{e_y}sin(\psi) + \vec{e_x}cos(\psi))\right) + & \\ & C_{10}Q_1^{0'}(cosh(\eta))sinh(\eta)cos(\vartheta) + & \\ & \widetilde{C_{11}}sin(\vartheta)\left(\vec{e_y}sin(\psi) + \right. & \\ & \left.\vec{e_x}cos(\psi)\right)Q_1^{1'}(cosh(\eta))sinh(\eta) & \\ \frac{\partial V_2}{\partial\vartheta} = & -\frac{\vec{B_0}a}{\mu_0}\left(\vec{e_z}cosh(\eta)sin(\vartheta) + \right. & \\ & \left. sinh(\eta)cos(\vartheta)\right. & \\ & \left.(\vec{e_y}sin(\psi) + \vec{e_x}cos(\psi))\right) - & \\ & C_{10}Q_1^0(cosh(\eta))sin(\vartheta) + & \\ & \widetilde{C_{11}}cos(\vartheta)Q_1^1(cosh(\eta)) & \\ \frac{\partial V_2}{\partial\psi} = & -\frac{\vec{B_0}a}{\mu_0}sinh(\eta)sin(\vartheta) & \\ & (\vec{e_y}cos(\psi) - \vec{e_x}sin(\psi)) + & \\ & \widetilde{C_{11}}sin(\vartheta)Q_1^1(cosh(\eta)) & \\ & (\vec{e_y}cos(\psi) - \vec{e_x}sin(\psi)) & \end{array} \tag{14}$$

where $\vec{e_x}$, $\vec{e_y}$ and $\vec{e_z}$ are the unit vectors in the coordinate directions.

Still (10) is valid for spheroids whose major semi-axis coincides with the z-axis. With a simple rotational operation finally the flux density for a spheroid with angles θ and ϕ can be obtained

$$\begin{array}{rcl}B_x & = & B'_x cos(\theta)cos(\phi) - B'_y sin(\phi) + \\ & & B'_z sin(\theta)cos(\phi) \\ B_y & = & B'_x cos(\theta)sin(\phi) + B'_y cos(\phi) + \\ & & B'_z sin(\theta)sin(\phi) \\ B_z & = & -B'_x sin(\theta) + B'_z cos(\theta)\end{array} \tag{15}$$

TWO STAGE RECONSTRUCTION OF THE UXO ORIENTATION

First Stage: Information from Field Signatures

As mentioned above, the reconstruction problem consists of determining 7 parameters, namely (x_0, y_0, z_0) — the location of the center of the prolate spheroid; (b, c) — the minor and the major semi-axes of the spheroid; and (θ, ϕ) the angles between the major semi-axis and the z-axis and the x-axis respectively.

Different to [1] not only the accuracy requirement but also the speed requirement is important in this work, hence the reconstruction problem will be solved abandoning stochastic methods. This, however, bears the possibility of getting stuck in a suboptimal point in the parameter space, hence a good starting point for the reconstruction is crucial.

In this section the question is going to be answered whether or not some of these parameters can be determined *a priori* by inspection of the magnetic field signature at the measurement plane.

For the following investigations an earth magnetic field of $|B| = 47.9\,\mu T$, $\theta_B = 30^o$ and $\phi_B = 45^o$ is assumed, which is approximately the earth magnetic field in Central Europe.

The major semi-axis of the spheroid is 1.5 m and the minor semi-axis is 0.2 m. The center of the UXO is located in a depth of 2 m and the measurement plane is 0.5 m above the ground.

In Fig. 2 - Fig. 4 the signatures (i. e. the magnetic field plot) for different UXO locations are given.

As can be seen in Fig. 2 - Fig. 4 some *a priori* information can be drawn from the magnetic field signatures.

Especially the B_z signature allows to determine the center of the spheroid in the xy-plane with acceptable accuracy, simply by calculating the middle point between the location of the maximum and the minimum in the B_z signature.

Additionally the angle ϕ can be calculated from the signature, since the angle of the directional vector from the minimum peak to the maximum peak is approximately equal to ϕ, provided that θ is neither zero nor 90^o.

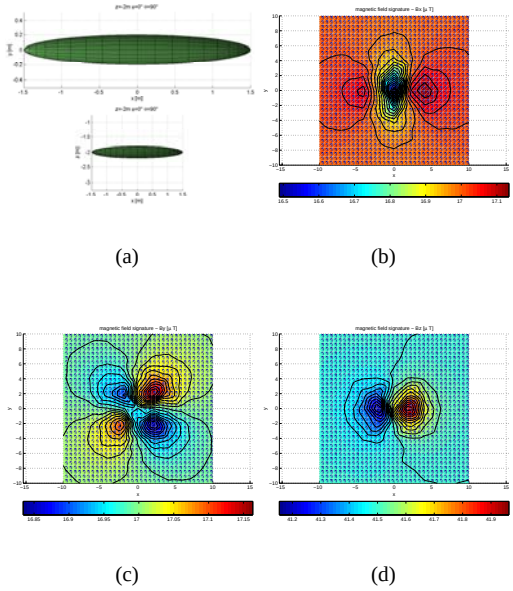

(a) (b)

(c) (d)

Figure 2: Prolate spheroid $\theta = 90^o$, $\phi = 0^o$: (a) orientation of the UXO in space, (b) B_x signature in height $0.5\,m$, (c) B_y signature in height $0.5\,m$, (d) B_z signature in height $0.5\,m$

Furthermore one can impose a reasonable equality constraint, namely that the fraction of the major semi-axis and the minor semi-axis is 2.5 (which is sensible for most UXOs).

With the *a priori* information and the assumption for the semi-axis, one ends up with 3 parameters to be reconstructed, namely the depth z_0, the angle between the z-axis and the major semi-axis of the spheroid θ and the minor semi-axis of the spheroid b.

In the following the reconstruction that is performed using the *a priori* information from the magnetic field signature and the assumption about the axis of the prolate spheroid will be called *coarse reconstruction*.

For practical reasons the requirements for the *course reconstruction* are that it should be fast (less than a minute on a 1GHz Pentium with 128 Mb memory) and that the location of the UXO should be found with an acceptable precision ($\pm$ 0.5 m). Furthermore the angles ϕ and θ should be found

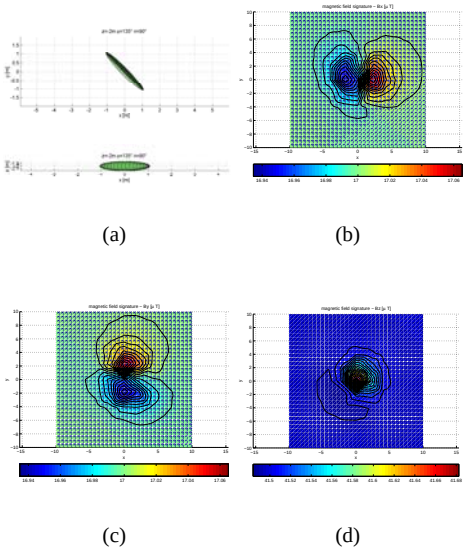

(a) (b)

(c) (d)

Figure 3: Prolate spheroid $\theta = 90^o$, $\phi = 135^o$: (a) orientation of the UXO in space, (b) B_x signature in height $0.5\,m$, (c) B_y signature in height $0.5\,m$, (d) B_z signature in height $0.5\,m$

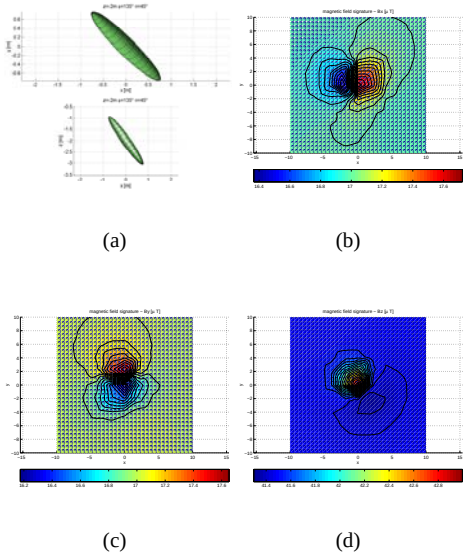

(a) (b)

(c) (d)

Figure 4: Prolate spheroid $\theta = 45^o$, $\phi = 135^o$: (a) orientation of the UXO in space, (b) B_x signature in height $0.5\,m$, (c) B_y signature in height $0.5\,m$, (d) B_z signature in height $0.5\,m$

with an error less than $\pm 10^o$ (the dimensions of the semi-axes of the spheroid are of minor interest at this stage). The *coarse reconstruction* leads to the values x_0^c, y_0^c, z_0^c, b^c, c^c, ϕ^c and θ^c.

Solution of the Inverse Problem for the Coarse Reconstruction

The inverse problem for the coarse reconstruction is formulated in a least squares sense for N measurement points

$$p_{opt}^c = \arg\min_{p^c} \sum_i^N \left(B_{z_i} - B_{z0_i}\right)^2 \qquad (16)$$

with

$$p^c = (z_0, \theta, b)\,T \qquad (17)$$

and p_{opt}^c being the optimal value for p^c.

One Gauss-Newton iteration for the step $t+1$ then is

$$p_{t+1}^c = p_t^c - \left(J^T J\right)^{-1} \left(J^T \left(\vec{B_z} - \vec{B_{z0}}\right)\right) \qquad (18)$$

with $\vec{B_{z0}}$ being a vector that contains all measured B_z values and $\vec{B_z}$ is the vector of calculated B_z values resulting from the spheroidal and

$$J_{i,j} = \frac{\partial B_{z_i}}{\partial p_j^c} \qquad (19)$$

being one entry of the Jacobi matrix.

Second Stage: Refined Reconstruction

The next (optional) stage of the reconstruction is to use the results from the *coarse reconstruction* as a starting guess for the so-called *refined reconstruction*, where all 7 parameters are reconstructed. The *refined reconstruction* parameters x_0^f, y_0^f, z_0^f, b^f, c^f, ϕ^f and θ^f are allowed to vary in the follow-

ing intervals

$$\begin{array}{rcccl} x_0^c - 0.5\,m & \leq & x_0^f & \leq & x_0^c + 0.5\,m \\ y_0^c - 0.5\,m & \leq & y_0^f & \leq & y_0^c + 0.5\,m \\ z_0^c - 0.5\,m & \leq & z_0^f & \leq & z_0^c + 0.5\,m \\ b^c - 0.2\,m & \leq & b^f & \leq & b^c + 0.2\,m \\ c^c - 0.5\,m & \leq & c^f & \leq & c^c + 0.5\,m \\ \phi^c - 10^o & \leq & \phi^f & \leq & \phi^c + 10^o \\ \theta^c - 10^o & \leq & \theta^f & \leq & \theta^c + 10^o \end{array} \qquad (20)$$

The refined reconstruction was carried out with a constrained Quasi-Newton method with a BFGS update for the Hessian matrix [6].

Reconstruction Results

The above mentioned procedure is applied to identify an UXO in 2 m depth. The signal that was used for reconstruction is the z-component of the magnetic flux density, which was measured on a square grid of 12 m $\times$ 12 m in 20 $\times$ 20 equally distributed points. The measurement grid is 0.5 m above ground. It is assumed that the location of the measurement points within the grid is known with high accuracy.

Additionally it has to be assumed, that the soil is not ferromagnetic.

The reconstruction was carried out applying a Gauss-Newton method, which minimizes the difference between the magnetic flux density that results from the prolate spheroid model and the measured flux density.

For the semi-axes of the spheroid a constraint was defined, such that the minor semi-axis is always smaller than the major semi axis.

The necessary first order derivatives have been calculated analytically.

The results in Table 1 have been obtained after 11 Gauss-Newton iterations (19 seconds on a 1GHz Pentium PC) for the *coarse reconstruction* process and after 62 iterations (3 minutes) for the *refined reconstruction*. The starting guess for the remaining parameters for the coarse reconstruction was $z_0 = -3\,m$, $b = 0.1\,m$ and $\theta = 10^o$.

Table 1: UXO reconstruction: true UXO dimensions and location (true), *coarse reconstruction* (reco1) and *refined reconstruction* (reco2)

	true	reco1	reco2
x_0 [m]	-1.0000	-1.2000	-1.0219
y_0 [m]	-0.5000	-0.9000	-0.4909
z_0 [m]	-2.0000	-2.2706	-2.0118
c [m]	1.0000	0.9773	1.0117
b [m]	0.3000	0.3909	0.2970
ϕ [degree]	35.0000	36.8699	34.4051
θ [degree]	80.0000	85.0000	80.0974

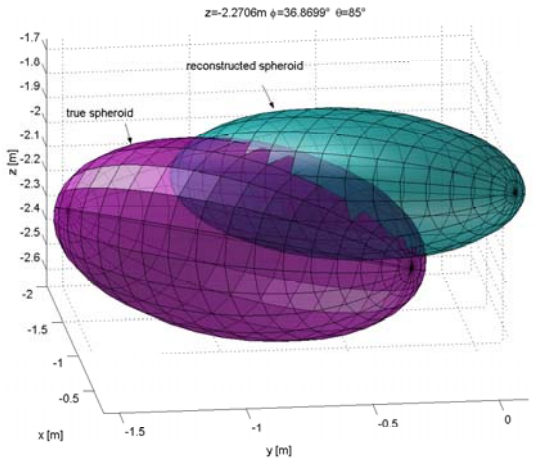

Figure 5: *coarse reconstruction*: Reconstructed spheroid (cyan) and true spheroid (red). The result has been obtained by reconstructing the depth z_0, the minor semi-axis of the spheroid b and the angle θ

WRONG ASSUMPTION FOR THE PERMEABILITY OF THE BOMB AND UNCERTAINTY IN SENSOR LOCATION

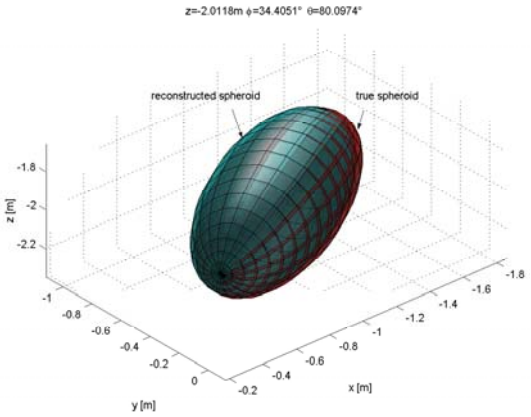

Figure 6: *refined reconstruction*: Reconstructed spheroid (cyan) and true spheroid (red). The result has been obtained by reconstructing all 7 parameters. The parameters were allowed to vary only within a small range around the values that have been obtained with the *course reconstruction*

First we study the effect for the reconstruction if the permeability of the spheroid in the mathematical model is different from the permeability of the true spheroid.

It is assumed in the following reconstruction that μ_r of the spheroid is 500, whereas the permeability of the true spheroid is 1000.

The reconstruction was again carried out in two steps: a course reconstruction with *a priori* data and 3 remaining parameters (reco 1) and a refined reconstruction with 7 parameters in a limited subspace according to (20) (reco 2). The results of the reconstruction with μ_r-uncertainty are given in Table 2.

Table 2: Reconstruction results for μ_r-uncertainty (μ_r^{true}=1000; $\mu_r^{assumed}$=500)

	true	reco1	reco2
x_0 [m]	-1.0000	-1.2000	-1.0327
y_0 [m]	-0.5000	-0.9000	-0.5038
z_0 [m]	-2.0000	-2.1604	-2.0009
c [m]	1.0000	0.9482	1.0226
b [m]	0.3000	0.3793	0.2927
ϕ [degree]	35.0000	36.8699	34.7013
θ [degree]	80.0000	84.5084	80.2398

For the results in Table 2 again the starting guess was $z_0 = -3\,m$, $b = 0.1\,m$ and $\theta = 10^o$; and as starting guess for reco 2, the result of reco 1 was chosen.

The result obtained from reco 2 is in very good agreement with the parameters of the true spheroid. Hence a wrong assumption for μ_r has little effect on the solution.

Next the effect on the reconstruction of uncertainty in the locations of the magnetic field sensors is examined.

In the following it is assumed that a sensor location in the x-y-plane is known with an error of $\pm\,6\,cm$.

Fig. 7 shows some of the true sensor locations (red) and the locations of the sensors that are used for the reconstruction (blue).

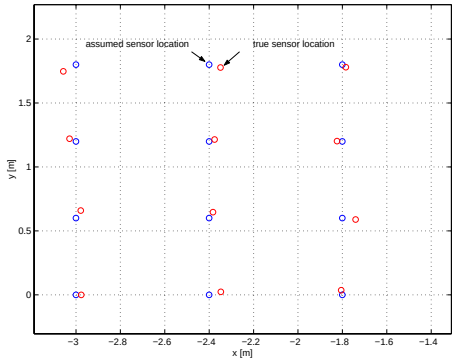

Figure 7: True sensor locations (red) and assumed sensor locations for the reconstruction (blue)

Once again the starting guess was $z_0 = -3\,m$, $b = 0.1\,m$ and $\theta = 10^o$. The results of the reconstruction are given in Table 3.

Table 3: Reconstruction results for uncertainty in sensor location of $\pm\,6\,cm$

	true	reco1	reco2
x_0 [m]	-1.0000	-1.2276	-0.9556
y_0 [m]	-0.5000	-0.8757	-0.5239
z_0 [m]	-2.0000	-2.2657	-2.0280
c [m]	1.0000	0.9667	1.0078
b [m]	0.3000	0.3867	0.3342
ϕ [degree]	35.0000	36.5284	35.5416
θ [degree]	80.0000	85.0000	84.1482

The results after reco 2 are in good agreement with the parameters of the true spheroid as well, however, it cannot be concluded that one could be too careless what the knowledge of the sensor locations is concerned. In the following an uncertainty of $\pm\,20\,cm$ in the sensor location was investigated, leading to the results in Table 4.

Table 4: Reconstruction results for uncertainty in sensor location of $\pm\,20\,cm$

	true	reco1
x_0 [m]	-1.0000	-1.2312
y_0 [m]	-0.5000	-0.7787
z_0 [m]	-2.0000	-3.4526
c [m]	1.0000	1.2500
b [m]	0.3000	0.5000
ϕ [degree]	35.0000	35.3770
θ [degree]	85.0000	85.0000

The results in Table 4 show that after reco 1 the results differ quite significantly from the true parameters, especially $z_0 = -3.4526\,m$ is completely out of scope, thus to perform reco 2 is useless in this case.

CONCLUSION

It has been shown in this section that a ferromagnetic UXO can be detected with high accuracy. Investigations have shown that the reconstruction results are quite insensitive to the assumption of the relative permeability of the spheroid in the mathematical model. However one has to take care what the knowledge of the sensor locations is concerned. It has been demonstrated that acceptable reconstruction results can be obtained with an uncertainty in the sensor locations of $\pm\,6\,cm$; however reconstruction fails with an uncertainty in sensor locations of $\pm\,20\,cm$, an error, which may appear very large but if one single mobile sensor is used and the location of the sensor is determined by GPS, this error is quite low.

Once again the main problem for magnetometer based UXO detection and reconstruction has to be mentioned: A non-ferromagnetic UXO is completely invisible to the reconstruction environment. In this case it is good practice to carry out UXO detection with other methods like GPR or EIM.

REFERENCES

[1] B. Brandstätter, Ch. Magele, C. Ragusa, M. Repetto, 'Identification of burried ferromagnetic Objects by means of different approaches', *Proceedings of the 5th International Workshop on Optimization and Inverse Problems*, Finland, 1998

[2] Bruce Barrow, H. Nelson,<'Collection and Analysis of Multi-Sensor Ordnance Signatures with MTADS', *The Environmental and Engineering Geophysical Society*, vol. 3, issue 2, p 71, June 1998

[3] Stephen J. Norton, Alan J. Witten, 'Target Parameter Estimation and Survey Design in Magnetometry', *The Environmental and Engineering Geophysical Society*, vol. 3, issue 3, p 147, September 1998

[4] Bruce Barrow, Nagi Khadr, and Robert DiMarco, Herbert H. Nelson, 'The Combined Use of Magnetic and Electromagnetic Sensors for Detection and Characterization of UXO', Proc. Symposium on the Application of Geophysics to Engineering and Environmental Problems SAGEEP 96, Keystone, CO, 1996.

[5] A. Salem, T. J. Gamey, D. Ravat, K. Ushijima, 'Automatic Detection Of UXO From Airborne Magnetic Data Using A Neural Network', Proceedings of SAGEEP, Denver, CO, March 2001

[6] R. Fletcher: *Practical Methods of Optimization*, Wiley, 1987